AFTER, an ASIC for the Readout of the Large T2K Time Projection Chambers.

P. Baron, D. Calvet, E. Delagnes, X. de la Broise, A. Delbart, F. Druillole, E. Mazzucato, E. Monmarthe, F. Pierre, M. Zito.

Abstract— **The T2K (Tokai-to-Kamioka) experiment is a long baseline neutrino oscillation experiment in Japan, for which a near detector complex (ND280), used to characterize the beam, will be built 280m from the target in the off-axis direction of the neutrino beam produced using the 50 GeV proton synchrotron of J-PARC (Japan Proton Accelerator Research Complex). The central part of the ND280 is a detector including 3 large Time Projection Chambers based on Micromegas gas amplification technology with anodes pixelated into about 125,000 pads and requiring therefore compact and low power readout electronics. A 72-channel front-end Application Specific Integrated Circuit has been developed to read these TPCs. Each channel includes a low noise charge preamplifier, a pole zero compensation stage, a second order Sallen-Key low pass filter and a 511-cell Switched Capacitor Array. This electronics offers a large flexibility in sampling frequency (50 MHz max.), shaping time (16 values from 100 ns to 2 μs), gain (4 ranges from 120 fC to 600 fC), while taking advantage of the low physics events rate of 0.3 Hz. Fabricated in 0.35 μm CMOS technology, the prototype has been validated and meets all the requirements for the experiment so that mass production has been launched at the end of 2007.**

Index Terms— **Mixed analog-digital integrated circuits, Front-end electronics, CMOS.**

I. INTRODUCTION

THe T2K (Tokai-to-Kamioka) experiment [1] is dedicated to the study of neutrino oscillations. An intense neutrino beam from the J-PARC (Japan Proton Accelerator Research Complex) facility in Tokai will be sent 295 km across Japan towards the Super Kamiokande detector in Kamioka in order to study how neutrinos change from one type to another. The ND280 detector complex, located at 280 m from the neutrino production target, will measure properties of the neutrino beams at the J-PARC site before the neutrinos have had a chance to oscillate into other flavors. This near detector complex consists of finely segmented detectors acting as neutrino targets and tracking detectors surrounded by a magnet to measure the neutrino beam energy spectrum, flux, flavor contents, and interaction cross-sections before the neutrino oscillation. One of the major parts of this detector is the tracker constituted by three Time Projection Chambers (TPC). These TPCs will measure the momenta of muons produced by

charged current interactions in the detector, and it will be used to reconstruct the neutrino energy spectrum. The outer dimensions of each TPC (Fig. 1) are roughly a 2.5 m x 2.5 m in the plane perpendicular to the neutrino beam direction, and 1 m along the beam direction.

Each TPC is read out at each of its extremity by micro pattern readout endplates using the bulk Micromegas technology [2]. This Micromegas detector is made of a segmented Printed Board Circuit (PCB), used as the anode, on top of which a stainless steel micromesh is integrated using
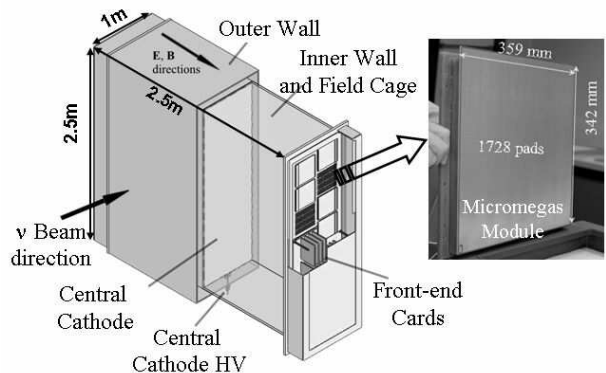

Fig. 1. Global view of a TPC and of a 36 cm x 34 cm Micromegas readout module.

photolithography techniques. Each TPC end-plate is made of 12 Micromegas modules of 36 cm x 34 cm. The readout anode of each module is pixelated in 1728 pads of 6.9 mm x 9.7 mm. The readout of the total 125,000 pads of the three TPCs implied therefore the design of dedicated readout electronics. As it fits in the area enclosed by the magnet, these front-end electronics have to be compact and low power.

II. OUTLINE OF THE TPC ELECTRONICS

The goal of the TPC detectors is to perform 3D tracking of charged particles and to measure their energy loss. For this purpose, the electronics will measure the charge collected by each pad. A centroid calculation will permit to determine X and Y coordinates for each point of the track, whereas the Z coordinate will be given by the drift time of electrons to the endplate of the TPC. To measure these parameters, for each particle spill (every 3.5 s), each pad signal will be recorded over duration slightly larger than the maximum TPC drift time (few tens of microseconds). The overall electronics architecture has been optimized to handle and concentrate the

resulting highly bursted data flow and to minimize cabling coming out from the detectors, taking benefit of the very low event rate (0.3 Hz in standard condition and up to 20 Hz for cosmic ray calibration). For this purpose, the electronics is based on an architecture derived from those developed for the former STAR TPC [3], but more compact and with better noise and power consumption performances, thanks to the use of modern technologies. The on-detector electronics, located inside the magnet, is based on a modular electronics unit, depicted in Fig. 2, reading one whole Micromegas module. This unit, connected directly to the anodes, is composed of 6 Front-End Cards (FECs) and one Front-End Mezzanine (FEM) card.
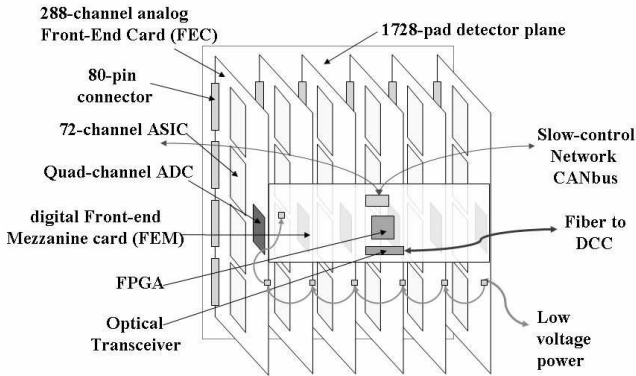

Fig. 2. TPC module readout electronics.

Each 288-channel FEC includes mainly input protection networks, 4 custom-made 72-channel "AFTER" front-end chips (ASIC For TPC Electronic Readout) and a commercial 12-bit quad-channel ADC. The ASIC collects and filters the detector signals and samples them continuously in an analog memory, based on a Switched Capacitor Array (SCA) until a trigger arrives. Then the analog data from all the channels of the chip is multiplexed towards one of the four channel of the external ADC achieving thus a first 72-to-1 data concentration.

The FEM is a digital electronics card that controls up to 6 FECs, gathers events digitized by the FECs, performs optionally pedestal subtraction and zero suppression, and sends data outside the detector through a full-duplex gigabit optical link. Outside the detector, 6 Data Concentrator Cards (DCC) aggregate the data of the TPC endplates and send event fragments to a merger computer that performs a final data reduction and communicates with the experiment DAQ system via a standard network connection.

III. THE AFTER ASIC

This section describes the architecture of the chip which has been optimized to match the main specifications and requirements reported in Table I. The required dynamic range is 10 bits. The chip gain can be selected among 4 values to adapt the measurement range to the maximum charge delivered by the detector. This charge is ten times the charge delivered by the detector for a Minimum Ionizing Particle

(MIP) that will depend on the detector parameters like gas mixture and voltage applied.

TABLE 1: MAIN REQUIREMENTS AND SPECIFICATIONS

Parameter	Value
Number of channels	72
Samples per channel	511
Dynamic Range	2 V / 10 MIPs on 12 bits
MIP charge	12 fC to 60 fC
MIP/Noise ratio	100
Gain	4 values from 4 mV / fC to 18 mV / fC
"Detector" capacitor range	20 pF -30 pF
Peaking Time	100 ns to 2 µs (16 values)
INL	1% 0-3 MIPs ; 5% 3-10MIPs
Sampling frequency	1 MHz to 50 MHz
Readout frequency	20 MHz to 25 MHz
Polarity of detector signal	Negative (T2K) or Positive
Test	1 among 72 channels or all

A. Architecture of the AFTER Chip

The AFTER chip (Fig. 3) is the central component of the FEC board. Defined before the final choice of the detector, it was developed to accommodate various kinds of detectors and gas mixtures. It can even operate with both signal polarities depending on the choice of few external components. It performs a first concentration of the data from 72 inputs to only one analog output connected to an external ADC.
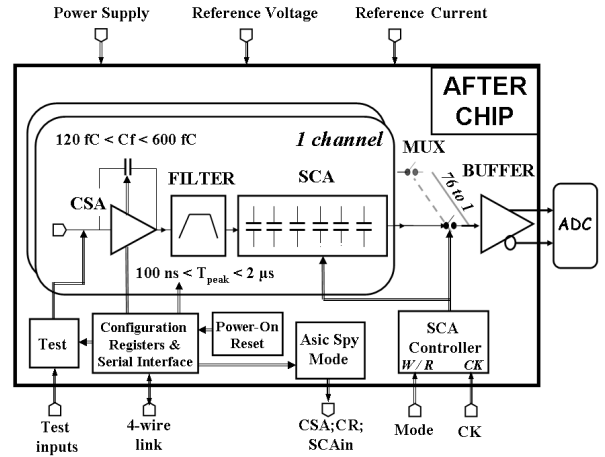

Fig. 3. Architecture of the AFTER chip.

Each channel comprises a front-end part dedicated to the charge collection and the shaping of the detector signal and a SCA that samples and stores the analog signal. Several parameters (gain, peaking time, test modes and chip control) are programmable, using a custom serial 4-wire link. Two inputs are provided for calibration and the functional test of the 72 channels.

B. Architecture of the Front-End Part of the Channel

The front-end part (depicted on Fig. 4) is composed of: a Charge Sensitive Amplifier (CSA), a Pole-Zero Cancellation (PZC) network, a second order low-pass filter and a Gain-2 amplifier. The CSA is based on single-ended folded cascode architecture [4]. It has been optimized for detector capacitances in the 20 pF - 30 pF range. The input transistor is a NMOS device (2000 µm / 0.35 µm) biased with an adjustable drain current in the 100 µA - 1 mA range. This current is set by an external resistance and can be remotely doubled via the serial link. The full charge range (120 fC, 240 fC, 360 fC or 600 fC) is defined by selecting the CSA feedback capacitor value (200 fF, 400 fF, 600 fF or 1 pF). The DC feedback of the CSA is achieved by an attenuating current conveyor [5] which is also used to realize the resistor setting the zero of the PZC stage. The PZC stage is used to cancel the long duration undershoots at the shaped output. It introduces a zero to cancel the low frequency pole of the CSA and replaces it by a higher frequency pole.

Associated with the PZC pole, the 2-complex pole Sallen-Key low-pass filter provides a semi-Gaussian shaping of the analog signal. We have limited the total number of poles of the shaper to three to minimize the number of amplifiers and thus the power consumption. The low frequency gain of the Sallen-Key filter is set by the ratio $(C_y+C_x)/C_y$ of the capacitors located in the negative feedback path of the amplifier. As C_x is double than C_y, this gain is equal to 3/2 setting a damping factor [6] equal to 0.75. The natural pulsation of the filter is defined by the values of the resistors (R_s) and capacitors (C_s) located in the positive feedback path of the amplifier. R_s and C_s are identical to the components setting the pole in the PZC stage. The peaking time at the shaper output can be set among 16 values (from 100 ns to 2 µs) by varying the value of Rs

both in the Sallen-Key and in the PZC stages. We have chosen this particular filter, rather than the well known third-order gaussian approximation described in [7] for the following reasons:

- The step responses of these two filters are very similar. The major exception is a larger overshoot of 0.8% for our filter instead of 0.025% .
- But, for a same peaking time, the 5%-occupation of the step response of our filter is 10% smallest. So that it has better double track resolution performances.
- For the same peaking time, the differences of the series and parallel noise coefficients of the two filters are smallest than 1%.
- The damping factor of the selected filter is defined by a ratio between two capacitors which is equal to two and then very predictable and very robust to mismatches.
- In our filter, the same resistors and capacitances are defining the poles of the PZC and the Sallen-Key filters. So that, the value of the overall gain is very robust against systematic errors in the resistor and capacitor values and mismatches.

The last amplifier adjusts the voltage dynamic range of the chain (Gain of -2) to drive the analog memory. This stage, as the Sallen-Key filter makes use of OTAs (RHV in Fig. 4) biased with few nanoamps current as low frequency feedbacks which define sub-kiloHertz low frequency poles.

C. The Switched Capacitor Array

The analog memory is based on a SCA structure using 4-switches memory cells similar to those described in [8]. It includes 72 effective channels plus 4 dummy channels (Gain-2 stage + SCA) which can be used for common mode or fix pattern noise rejection. A SCA channel is made of 511
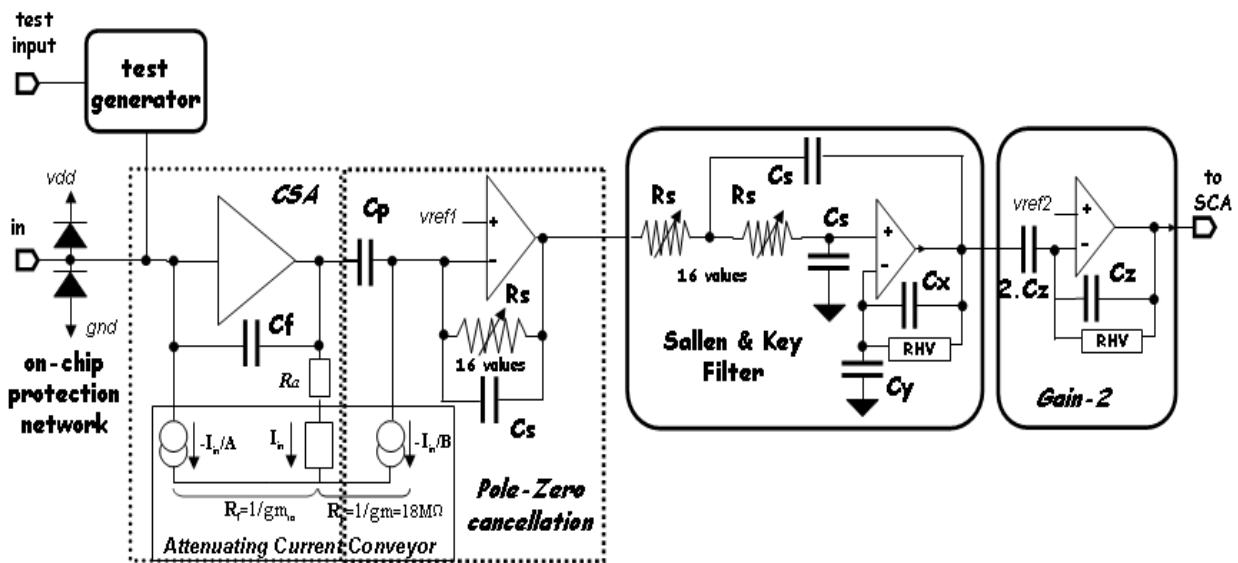

Fig. 4. Architecture of the front-end part of the channel.

memory cells and a readout-amplifier. Each SCA channel operates as a 511-cell circular analog buffer in which the signal coming out from each analog channel is continuously sampled and stored at a F_{wck} sampling rate (up to 50 MHz). Depending on the gas drift velocity, this frequency can be adjusted in order to cover the maximum TPC drift time with the 511 samples.

The sampling is stopped by the FEM when it receives an external trigger signal. Then, the 76 x 511 analog samples stored in the chip are read back and digitized at the readout clock rate of 20 MHz. This reading operation (Fig. 5) is performed time slice by time slice, starting from the oldest sample. For each of the 511 time slices, the read amplifiers are first reset during one readout clock cycle. Then all the 76 storage capacitances of a column corresponding to the same sampling time are read simultaneously by the 76 read amplifiers. Two more readout clock periods are required for the stabilization of the analog data at the read amplifier outputs. During these 3 first clock cycles, the chip output delivers a "reset" level. Afterward, the outputs of the 76 read amplifiers are successively multiplexed towards the output analog buffer. At the end of the readout phase, the digital address of the last column read is converted into a series of analog samples. This address can be analyzed offline for control purpose. The readout of the full memory takes 2 ms, but it is possible to read only part of the 511-cell SCA.

The on-chip analog fully-differential buffer drives one of the 4 inputs of the external ADC (Analog Devices AD9229). This buffer is designed to settle to 0.1% within 25ns (half read clock period). The input and output common mode voltages are adjusted with external passive components (same values for all chips).
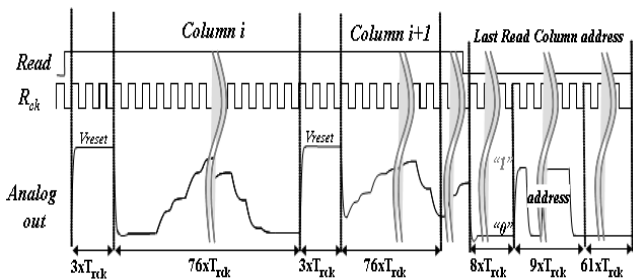

Fig. 5. Chronogram of the SCA read phase.

D. Chip Manufacturing, Layout and packaging.

The AFTER chip has been fabricated in a 0.35 μm CMOS AMS process. The chip integrates 400,000 transistors, and as shown in Fig. 6, its area (7.8 mm × 7.4 mm) is mainly dominated by the SCA. The channel input pads are located on the right and left sides of the chip by group of 36 in order to make the chip assembling easier in a standard 160-pin LQFP plastic package. The main digital blocks, including the SCA controller, the clocks buffering and the chip configuration interface are located in the bottom part of the chip.
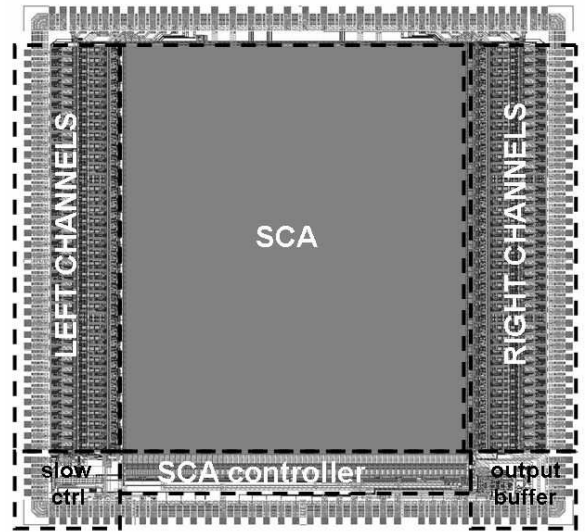

Fig. 6. AFTER chip layout.

IV. TEST RESULTS

Nearly two hundred chips have been characterized using test boards permitting also to validate the final FEC and FEM architectures. As in its final use in the experiment, the 12-bit ADC range was set to 2 V so that its LSB value was corresponding to 0.49 mV.

All the chip functionalities and its various modes of operation have been fully validated. The measured chip power consumption ranges from 6.2 mW to 7.5 mW per channel, depending on the bias current of the CSA (400 μA or 800 μA).

A. Signal Shape and Baseline Spread.

Fig. 7 shows the response of the AFTER chip to mid-range pulses injected through the test input for 4 different shaping times, and recorded using a 50 MHz sampling frequency.
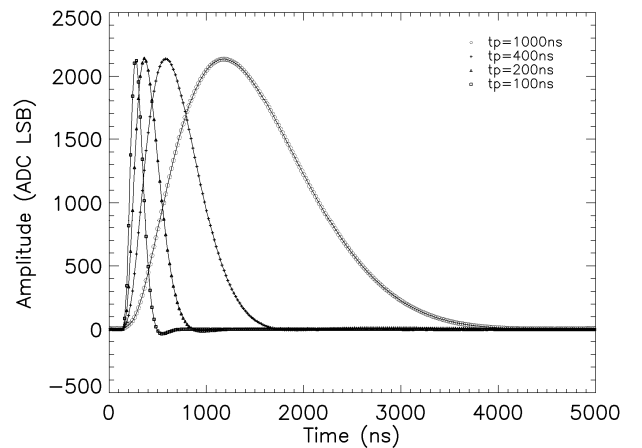

Fig. 7. 60 fC test pulses recorded by AFTER (120 fC range).

As expected, this response exhibits a small undershoot. Its magnitude is 1.5% of the maximum for the 100 ns peaking time because of parasitic elements and is 0.8% or less for the

other peaking times. The timing parameters of the pulses measured for various peaking times, reported in Table II, are consistent with the simulation results. In this table, T_{peak} is the signal rise time measured from 5% of the full amplitude to the peak, T_{fall} is the signal fall time measured from the peak to 5% and T_{FWHM} is the signal width measured at 50% of the signal amplitude.

TABLE II: MEASURED TIMING PARAMETERS OF THE SHAPED PULSES

Shaping time (ns)	T_{peak} (5%-100%) (ns)	T_{fall} (100%-5%) (ns)	T_{FWHM} (ns)
100	111	182	150
200	185	552	287
400	387	823	631
1000	893	2118	1529
2000	1776	4037	2953

Inside a chip, the channel-to-channel baseline spread is within 160 to 300 LSBs peak-to-peak. The spread of the baselines over 50 chips is 360 LSBs peak-to-peak. These values are in good agreement with Monte-Carlo simulation results showing that this spread is dominated by the contribution from the SCA readout. Individual analog baseline adjustment is not required and the mean baseline will be set to 200 LSBs. As the total dynamic range is 4096 LSBs the maximum effect of this spread will be a loss of dynamic range smaller than 10%.

B. Transfer Function and Linearity.

The AFTER chip has been characterized using pulses generated by a 14-bit DAC housed on the test board and injected to the chip calibration input through a calibrated external capacitance. The channel gain has been extracted from characteristics as the one plotted in Fig. 8 which was obtained for a 100 ns peaking time and the 120 fC range. These measured values are very close to the simulated ones.
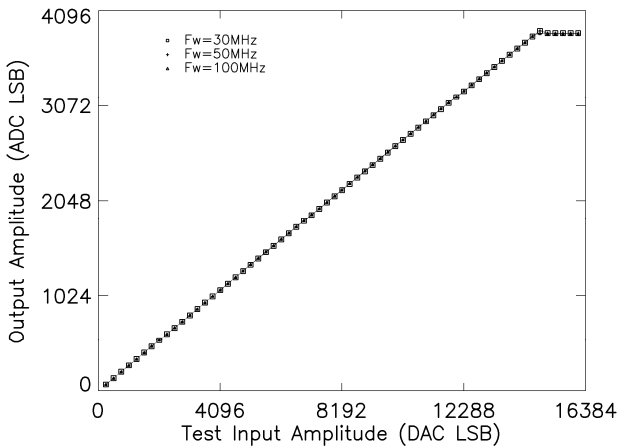

Fig. 8. Output amplitude versus test pulse amplitude measured for three SCA write frequencies (120fC range, 100ns peaking time).

They are summarized in Table III, for the four charge ranges available and for a shaping time of 100 ns that is the most sensitive one. Their spread measured over 122 chips is less than 2% rms. The CSA open loop gain, calculated from the measured transfer function versus input capacitance characteristic, is 3000. This is smaller than the 3700 simulated value. It can be partially explained by an overestimation of the MOS simulated output impedances. Actually, on individual transistors using the same technology, we noticed discrepancy up to 15% between measured and simulated output impedances.

TABLE III: AFTER TRANSFER FUNCTION (100NS SHAPING TIME)

Range (fC)	Simulated value (mV / fC)	Measured value (mV / fC)	spread over 120 chips (% rms)
120	18.5	18	1.7%
240	9.9	9.7	1.25%
360	6.6	6.67	1.15%
600	4.05	4.1	1.1%

The chip Integral Non-Linearity (INL), calculated as the normalized residues to a linear fit of the measured gain is smaller than 1.2% over the full chip dynamic range for the 120 fC range and 100 ns peaking time (Fig. 9), which is the most unfavorable configuration. For a 2 μs peaking time, the INL is improved to less than 0.5%. For all configurations, the INL is better than the 5% specification.
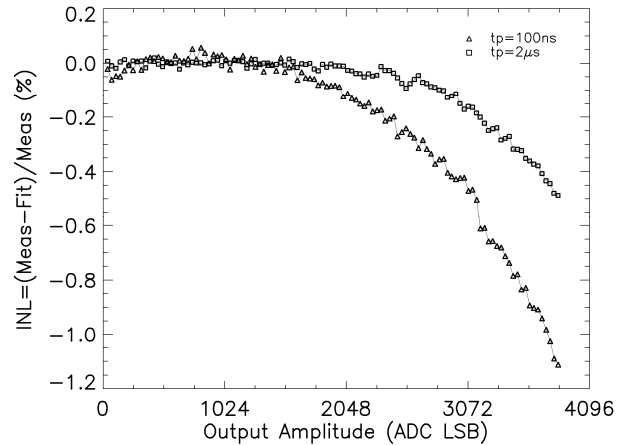

Fig. 9. Integral Non Linearity versus output amplitude for 100 ns and 2 μs peaking times (120 fC range).

Although the chip has been designed for a 50 MHz maximum SCA sampling frequency, it has also been characterized at higher frequencies. As shown in Fig.10, pulses sampled at 50 MHz and 100 MHz can be perfectly superimposed. The chip gain (Fig. 8) and the non-linearity curves (Fig. 11), measured at 30 MHz, 50 MHz and 100 MHz, are exactly the same. This shows the large speed margin of operation of the chip.
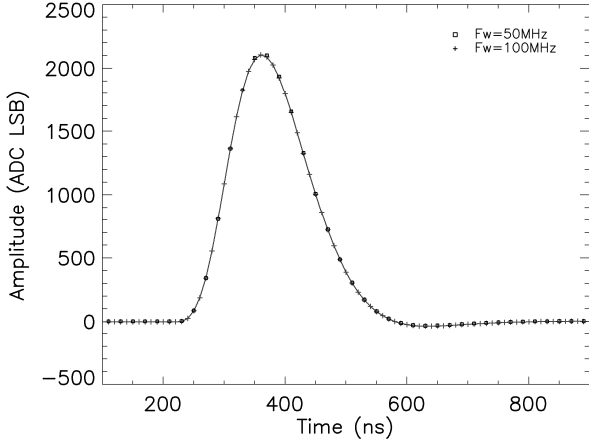
Fig. 10. Same single shot test pulse sampled at 50 MHz and 100 MHz (100 ns peaking time).
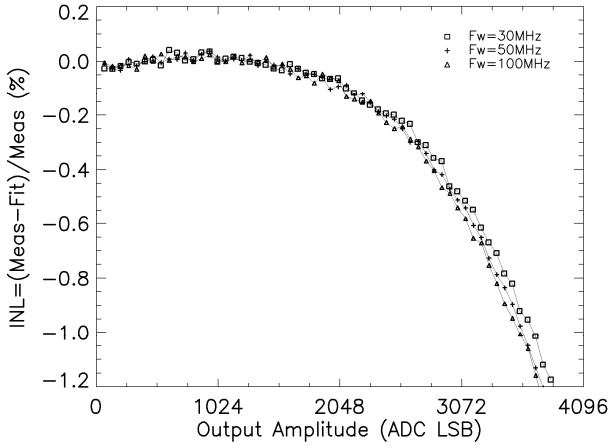

Fig. 11. Integral Non Linearity versus output amplitude for 100 ns peaking time, 120 fC range measured for three sampling clock frequencies.

C. Chip Noise.

The chip Equivalent Noise Charge (ENC) has been measured for the various available peaking times and different input capacitors. The ENC can be theoretically expressed as the quadratic sum [4]:

$$ENC^2 = \frac{\alpha^2(I_{csa}) \cdot (C_0 + C_{in})^2}{t_p} + \gamma^2 \cdot (C_0 + C_{in})^2 + \beta^2 \cdot t_p + D^2 \quad (1)$$

In (1), α stands for the series noise contribution (depending on the input transistor bias current), C_0 is the intrinsic input capacitor of the preamplifier, C_{in} is the added capacitor at the preamplifier input, t_p is the peaking time of the shaped signal, γ stands for the 1/f noise contribution, β stands for the parallel noise contribution and D is the second stage noise contribution. The parameters of this expression have been extracted by fitting the measured data for the four charge ranges of the chip, and for two CSA bias currents. Both the ENC measured values and the fitted curves, which perfectly match the measurements, are shown in Fig. 12 for the 120 fC

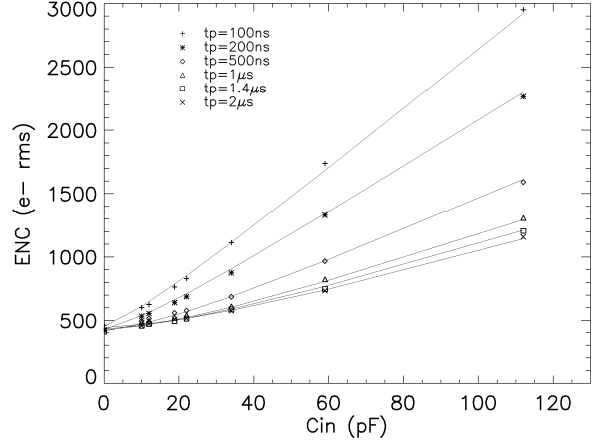range. The extracted noise parameters are summarized in Table IV.

Fig. 12. ENC versus input capacitance for different peaking times (120 fC range, I_{CSA}=800 µA). Symbols represent measurements, while lines represent fit results.

As expected, the parallel noise is negligible and the second stage noise value scales with the charge range. This latest appears to be shared equally between SCA and shaper contributions. The 10 pF intrinsic input capacitor C_0 value is 3 pF larger than the simulated one. This extra capacitor is compatible with those added by the plastic package. The series noise contribution is 10% larger than in simulation and is independent of the range. For 800 µA bias current, it corresponds to a 1.1 nV/Hz$^{1/2}$ CSA input transistor thermal white noise density. As expected, the 1/f noise is nearly independent of the current and of the charge range. However, its value is 80% higher than expected from simulation results. Fortunately, this unexplained excess noise has nearly no impact for the T2K experiment application for which the shaping time will be in the range of 200 ns to 400 ns.

TABLE IV: EXTRACTED NOISE PARAMETERS (QUADRATIC EXPRESSION)

Parameter	120 fC	240 fC	360 fC	600 fC	Unit
α(400 µA)	246	250	253	254	$e\text{-}.ns^{1/2}.pF^{-1}$
α(800 µA)	197	198	198	194	$e\text{-}.ns^{1/2}.pF^{-1}$
γ(400 µA)	6.6	6.6	6.9	8	$e\text{-}.pF^{-1}$
γ(800 µA)	6.66	6.9	7.5	8.6	$e\text{-}.pF^{-1}$
β	0	0	0	0	$e\text{-}.ns^{-1/2}.pF^{-1}$
C_0	10	10	10	10	pF
D	385	730	1070	1760	$e\text{-}$

For users' convenience, it is usual to approximate linearly the ENC versus C_{in} characteristic. Linear parameterization, valid only for input capacitances in the 15 pF - 40 pF range, is given in Table V for the four charge ranges and various peaking times, in the case of a 800 µA CSA bias current.

TABLE V: EXTRACTED NOISE PARAMETERS (LINEAR APPROXIMATION)

		100 ns	200 ns	500 ns	2 µs	Unit
120 fC	*Offset*	*350*	*370*	*415*	*404*	*e-*
	Slope	22.2	14.6	7.8	5.3	*e-/pF*
240 fC	*Offset*	*690*	*700*	*775*	*750*	*e-*
	Slope	13	8.5	4.5	3.1	*e-/pF*
360 fC	*Offset*	*1015*	*1050*	*1135*	*1092*	*e-*
	Slope	10.7	5.6	3	2.8	*e-/pF*
600 fC	*Offset*	*1700*	*1740*	*1817*	*1780*	*e-*
	Slope	6.5	3.2	3.3	1.8	*e-/pF*

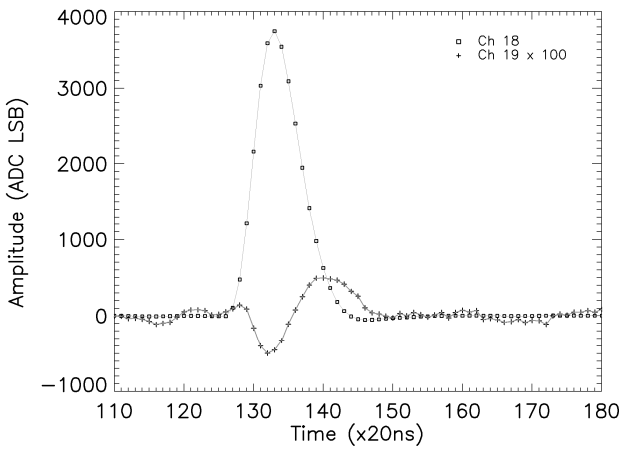## D. Crosstalk inside the Chip.

Fig. 13. Full dynamic range test input signal pulsed on channel 18 and crosstalk signal recorded on the neighbour channel 19, magnified by 100. (120 fC range, 100 ns peaking time).
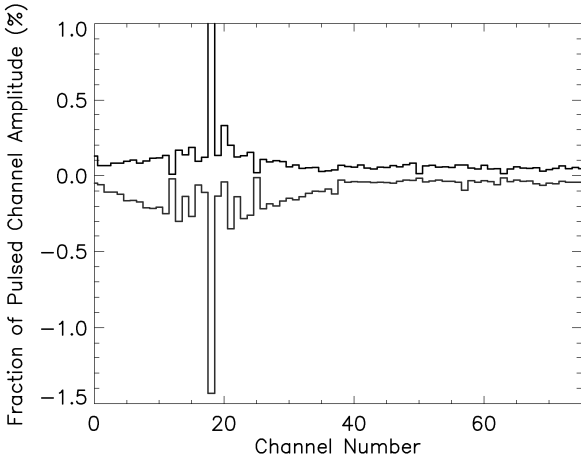

Fig. 14. Relative amplitudes (negative and positive) measured on all the channels of a chip referred to the amplitude of the pulsed (18) channel (100 ns peaking time, 120 fC range).

Crosstalk between channels in a TPC must be minimized as it deteriorates both the charge and position resolution. To measure it, a large amplitude test signal is injected in a single channel whereas the others are recorded. As shown in Fig. 13 the crosstalk signals are differentiated. For the 120 fC range and 100 ns peaking time, the crosstalk magnitude, plotted in

Fig. 14, is smaller than +/- 0.4% and at first order inversely proportional to the distance of the pulsed channel. The Crosstalk measured for other peaking times and ranges are similar. This crosstalk is intrinsic to the chip and does not take into account couplings at the detector level.

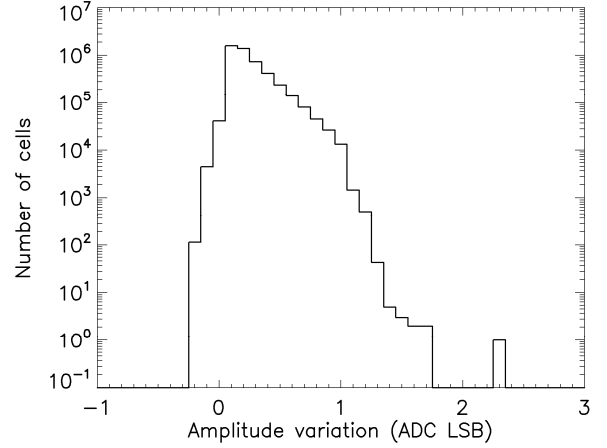## E. Effect of Leakage Current in the SCA.

Fig. 15. Distribution of the voltage droop on storage cells after a 2 ms storage time.

As the readout of the SCA takes 2 ms, the analog data stored in capacitors can be corrupted by leakage currents. The leakage effect has been characterized by varying the time between the write and read operations. As the effect of leakage current for a 2 ms storage time was too small to be measured accurately, measurements have been performed for a 35 ms storage time. The values obtained for 35 ms have been divided by 17.5 to extrapolate the effect corresponding to a 2 ms storage time. The voltage droop distribution measured over all the cells of 122 chips is plotted in Fig. 15. It is very asymmetric, with a mean value of 0.19 LSB. Nearly all the cells (99.95%) are exhibiting less than 1 LSB droop (corresponding to a 55 fA current) and the maximum measured droop is 2.2 LSB. For a worst case cell with 1 LSB droop, read randomly within a 2 ms interval, the readout voltage spread will be 0.29 LSB rms which is negligible compared to the 2.5 LSB rms second stage noise. The leakage current will be measured anyway during production tests so that chips with droop larger than 1 LSB within 2 ms will be rejected.

F. Yield.

200 AFTER ASICs coming from a single MPW run have been tested to equip a first module of the T2K TPC using the test bench that will be used for the full production. The measured yield is 73%. The bad chips are mainly rejected because a single or few faulty SCA storage cells.

A. Noise measurements of the chip mounted on the FEC.

On the FEC, each AFTER chip is associated to a connector and each signal input is ac-coupled to the anode and protected against detector sparks by the network depicted on Fig. 16. According to their specifications, the ESD protections integrated in the AFTER chip should be sufficient to protect the chip against the detector discharges which are limited by the 220 pF coupling capacitors. But as these protections have not been qualified yet with Micromegas detectors, two external BAV 99 diodes have been added at the chip input. The PhotoMOS, common to a group of 144 channels (2 AFTER chips) permits to disconnect remotely this group of channels in case of short circuit in the detector.
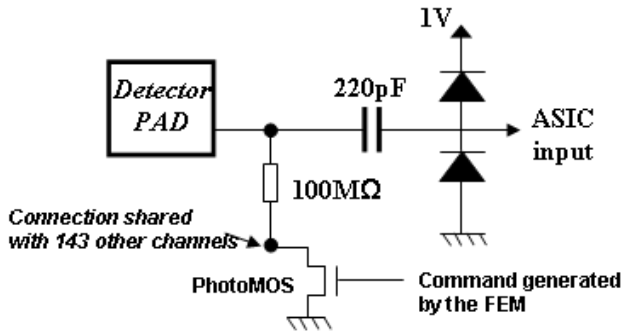

Fig. 16. AC-coupling to the detector and external protection network against sparks.
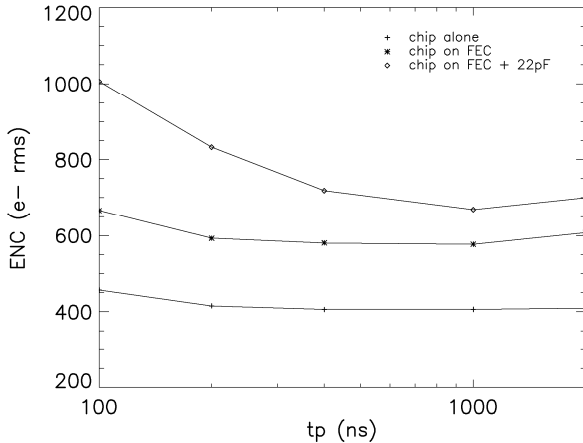

Fig. 17. Comparison of the ENC versus peaking time characteristic for the chip alone, mounted on the FEC and with extra 22 pF to simulate the detector (120 fC range, CSA bias current= 800 µA).

As shown on Fig. 17, the routing capacitance and all the external components increase the noise. An ENC measurement performed with extra 22 pF capacitors, simulating the detector, connected to each FEC input is reported in the same figure. In the worst case, for a peaking time of 100 ns, the ENC is 1000 e- rms. It is reduced to 850 e- rms in the 200 ns - 400 ns range, planned for the T2K operation.
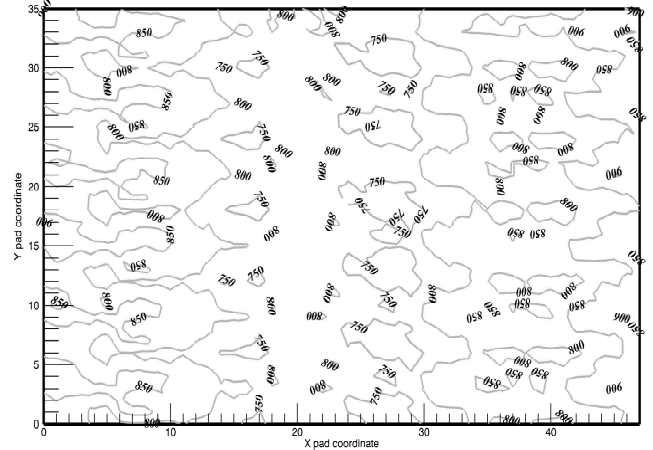
B. Noise Measurements with detectors.

Fig. 18. ENC map measured with a Micromegas detector. (100 ns peaking time, 120 fC range, 800 µA CSA bias current).

FECs have been mounted on a prototype Micromegas endplate. Fig. 18 shows a map of the ENC in the detector measured in the 120 fC range for the worst case 100 ns peaking time. The mean ENC over the detector is 810 e- rms with a spread of +/- 100 e- rms. The noise spread between channels, which presents a very regular pattern is mainly due to differences in routing on the detector from the pad to the connector, and therefore in parasitic capacitances. The detector capacitance value has been evaluated from these noise measurements. Its mean value is 12 pF with a minimum of 7 pF and a maximum of 17 pF, quite smaller than our estimations. Under these conditions the chip dynamic range is close to 10 bits.
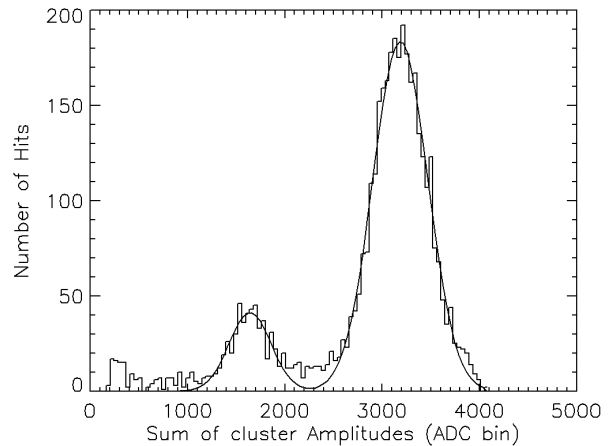
C. Measurements with particles.

Fig. 19. ^{55}Fe Spectrum acquired with AFTER (200 ns peaking time, 120 fC range, 20 MHz sampling frequency).

A Micromegas detector, read by AFTER chips, has been used to detect photons from a ^{55}Fe source. During data taking, noise levels were very stable and similar to those obtained in

the electronics laboratory. The spectrum (Fig. 19), measured with a 200 ns peaking time on the 120 fC range exhibits a very good 8.5% resolution for the 5.9 keV line, limited by the detector itself. Because of ac coupling between the detector and the electronics, a crosstalk corresponding to the ratio of the interpad capacitance over the ac-coupling capacitance is expected in addition to the intrinsic crosstalk in the AFTER chip reported in section IV.D. This has been evaluated using the data obtained with the ^{55}Fe source. First, the events hitting only a given pad were selected. The charges measured on two neighbour pads surrounding the hit pad are reported as a function of the charge of the central pad in Fig. 20. This graph shows a strong correlation between the charges measured on the two pads giving the evidence of a 1.2% crosstalk effect. This is consistent with a 2.5 pF parasitic capacitor between neighbour detector channels. This crosstalk magnitude varies from pad to pad but is always smaller than 1.2%, which is an acceptable value for T2K. The charge distribution measured on a neighbour pad, plotted in Fig. 21, shows a clear image of the source spectrum measured on the main pad (with charge scaled down by a factor 80). The charge resolution measured on this crosstalk spectrum is still good: 12% rms corresponding to 750 e- rms. This value includes both the detector resolution and the noise contribution. This proves the capability of the system to detect and measure small charges with a good accuracy.
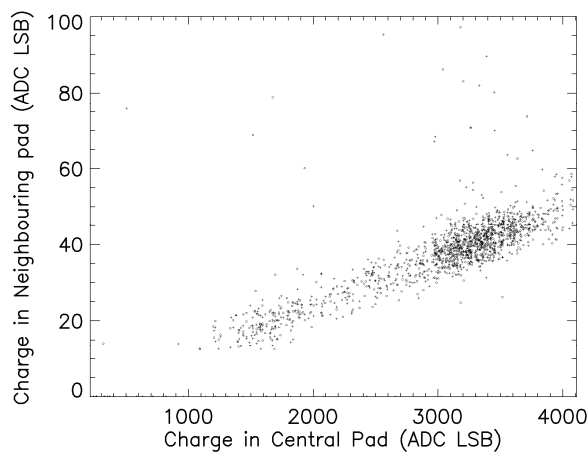

Fig. 20. Correlation graph between charges measured on two neighbour pads and charge on the main pad.

A Micromegas endplate detector, fully instrumented with AFTER electronics (including 6 FECs and one FEM), has also been tested in September 2007 with cosmic rays in the former HARP [9] field cage at CERN. The detector and its very compact electronics have operated continuously for two weeks. Noise levels were similar to those measured in-lab and were very stable. These tests and the associated results are discussed in [10].
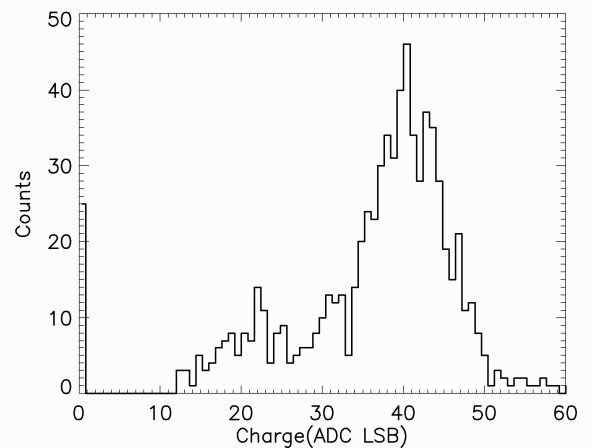

Fig. 21. Charge distribution measured for a neighbour pad.

VI. CONCLUSION

AFTER, a low noise front-end ASIC has been designed to read the endplate detector of the TPC of the T2K experiment. This very versatile circuit has been extensively tested and characterized. It fulfils the T2K experiment requirements and exhibits a noise of 800 e- rms for a 100 ns peaking time when connected to the detector, with a power consumption of less than 8 mW/channel. About 4000 AFTER chips have been manufactured for the T2K experiment at the end of 2007. Its low cost and its large number of tuneable parameters make it useable for other experiments with low rates or for detector testing.

REFERENCES

[1] Y. Itow, et al., hep-ex/0106019.
[2] J. Bouchez, et al., "Bulk Micromegas detectors for large TPC applications", Nucl. Instrum. Methods, vol 574 pp. 425-432, 2007.
[3] S.R. Klein et al., "Front end electronics for the STAR TPC", IEEE Trans. Nucl. Sci., Vol. 43, No. 3, pp 1768-1772, 1996.
[4] V. Radeka, P. O'Connor, "IC Front Ends for Nuclear Pulse Processing", IEEE NSS98 Short Course, Toronto.
[5] E. Delagnes et al., "SFE16, a low noise front-end integrated circuit dedicated to the read-out of large Micromegas detectors", IEEE Trans. Nucl. Sci., Vol. 47, No. 4, pp 1447-1453, 2000.
[6] P. Allen, D. Holberg, CMOS Analog Circuit Design, Oxford University Press, 1987.
[7] S. Ohkawa, M. Yoshizava, and K. Husimi, "Direct synthesis of the Gaussian filter for nuclear pulse amplifiers," Nucl. Instrum. Meth., vol. A138, pp. 85–92, 1976.
[8] D. Breton, J. Ardelean, E. Auge, R. Bernier, M. Bouchel, B. Lavigne, G. Martin-Chassard, E. Plaige, J. J. Veillet, E. Delagnes, and M. Huet, "A 16 bit-40 Mhz readout system based on dual port analog memories for LHC experiments," in Proc. 2nd Workshop on Electronics for LHC Experiments, Balatonfüred, Hungary, Sep.23–27, 1996, pp. 88–96.
[9] G. Prior, "The HARP time projection chamber", Nuclear Physics B - Proceedings Supplements, Volume 125, pp 27-42.
[10] E. Mazzucato et al., "Large bulk-Micromegas detectors for TPC applications in HEP". Nuclear Science Symposium Conference Record, 2007. NSS '07. IEEE Volume 6, Oct. 26 2007-Nov. 3 2007 pp 4640 - 4644